Abbreviations and Acronyms

ASME	American Society of Mechanical Engineers
ASME Code	ASME Boiler and Pressure Vessel Code
ASNT	American Society of Nondestructive Testing
AWS	American Welding Society
BWR	boiling water reactor
BWRVIP-03	BWR Vessel and Internals Project-3
CCTV	closed-circuit television
COD	crack opening displacement
CRDM	control rod drive mechanism
EPRI	Electric Power Research Institute
EVT	enhanced visual testing
IEEE	Institute of Electrical and Electronics Engineers
IGSCC	intergranular stress corrosion cracking
ISI	inservice inspection
ISO	International Organization for Standardization
LED	light-emitting diode
MTF	modulation transfer function
NDE	nondestructive examination
NRC	U.S. Nuclear Regulatory Commission
PNNL	Pacific Northwest National Laboratory
PWR	pressurized water reactor
RMS	root mean square
SCC	stress corrosion crack
SRCS	sensitivity, resolution, and contrast standard
UT	ultrasonic testing
VT	visual testing

1 Introduction

Visual testing (VT) is widely used as a primary inspection technique or to provide complementary information for other, more indirect nondestructive examination (NDE) methods. The human eye is highly adept at detecting small features or irregularities on the surfaces of materials, and direct VT, if applied under specific parameters, with appropriate optical tools and lighting, can exhibit highly reliable inspection results. Many VT applications use remotely operated video camera systems due to factors such as the location, size, and geometry of the parts or adverse environments surrounding the surfaces to be inspected. Because VT appears to be fundamentally simple and straightforward, and remote VT systems are convenient to deploy for periodic inspections, greater reliance is being placed on VT to determine the structural integrity of nuclear power plant components. However, the variables associated with VT personnel and equipment are often times not well defined. A better understanding of the effects of the variables on VT is required in order to determine their overall capabilities and limitations in detecting the targeted degradation.

In the commercial nuclear power industry, remote VT is used to examine components in the primary coolant system, including internal surfaces of the reactor pressure vessel and core support structures. These examinations are conducted either as part of an established inservice inspection (ISI) program required by Title 10, Part 50 of the *Code of Federal Regulations* or under licensee regulatory commitments such as the Boiling Water Reactor Vessels Internals Project (BWRVIP). Examinations conducted as part of an ISI program are performed in accordance with Section V and Section XI of the American Society of Mechanical Engineers Boiler and Pressure Vessel Code (ASME Code). The examinations performed in accordance with the BWRVIP adhere to the 150+ guidance documents that have been developed since the program's inception. Implementation variables such as the frequency of examinations, visual resolution, lighting parameters, acceptance criteria, and examiner qualifications are detailed in the ASME Code, Sections V and XI. The U.S. Nuclear Regulatory Commission (NRC) reviews and approves applicable ASME Code Editions for use at operating nuclear plants and ensures that ISI programs comply with NRC-approved ISI programs. The NRC also reviews and approves the requisite BWRVIP documents, and the NRC and the Institute for Nuclear Power Operations (INPO) routinely audit the plants to ensure compliance. Current ISI programs at operating reactors rely heavily on NDE to detect the presence of service-induced degradation that may lead to a breach of the pressure boundary or affect structural integrity; remote VT is one in a suite of NDE techniques that are deployed for this purpose.

The materials used in the design of safety-related components at commercial operating plants are robust; they were selected to provide good corrosion resistance, high strength, and fracture toughness. The most advanced forming and welding processes available were used under the auspices of high quality control programs during the fabrication of important components. Operating and residual tensile stresses are usually highest on the surfaces of the components near structural discontinuities such as welds or thickness transitions. For these reasons, it is commonly believed that service degradation will be initiated on the surfaces (not from embedded fabrication flaw growth) and will most likely occur first on the internal surfaces exposed to environments that could accelerate flaw initiation and growth. Therefore, in many cases, known degradation processes are expected to result in crack initiation on the internal surface of safety-related system components. For remote VT to be considered effective, inspection systems and implementation practices must be capable of detecting small cracks before they grow to a size that could challenge the leak-tightness of the pressure boundary.

To reduce some of the burden associated with ISI, the U.S. nuclear industry has increasingly been developing options to volumetric examinations (e.g., ultrasonic or radiographic testing) and surface examinations (e.g., electromagnetic, liquid penetrant, or magnetic particle testing) for certain components in commercial nuclear power plants by implementing remote visual tests. The advantages of using remote VT are that these tests generally involve much less radiation exposure and reduced inspection times than do the current volumetric and surface techniques. Because of geometry considerations, VT is used for some components because transducer access is limited or not possible. In some cases, the industry has proposed to perform "enhanced" remote visual examinations as alternatives to existing volumetric and/or surface tests.[1] This enhancement is based on the ability of the system to resolve a wire 12 μm (0.0005 in.) in diameter, intended as a baseline system calibration. With regard to using VT rather than volumetric methods, an analysis of all the pertinent issues is needed relative to the reliability of remote VT in determining the structural integrity of reactor components.

This report expands on the work performed earlier by Pacific Northwest National Laboratory (Cumblidge et al. 2004; NUREG/CR-6860) for the NRC. It is intended to provide a basis for describing the technical issues that must be addressed when applying remote VT to detect cracking phenomena by highlighting the inherent capabilities and limitations associated with current system deployment. The work has been aimed at nuclear power plant components; however, these issues exist for all industries where remote VT is expected to reliably detect small flaws.

Section 2 provides important background information on visual testing, defines terms, and explains concepts that will be used later in the report; it also covers the characteristics of flaws found in stainless steels and nickel alloys as well as a representative range of the sizes of tolerable flaws in nuclear reactors. Section 3 describes the experimental apparatus used to conduct the parametric studies and the laboratory tests on commercially used remote visual testing cameras. Section 4 presents and discusses the results of the parametric study. Section 5 describes the results of the laboratory tests on the commercially available camera systems that were used to detect a series of cracks. Section 6 describes the conditions found in commercial nuclear reactors. The visual testing results are described in Section 7, and conclusions are given in Section 8.

(1) Dorman WJ. Correspondence, Carolina Power and Light to U.S. Nuclear Regulatory Commission. "Brunswick Steam Electric Plant, Units 1 and 2, Docket Nos. 50-325 and 50-324, License Nos. DPR-71 and DPR-62, Request for Approval of Revised Relief Request for the Third 10-Year Inservice Inspection Program," August 7, 2000.

2 Background

As reactor components in a nuclear power plant are generally maintained underwater and/or reside in high radiation fields, remote examination with watertight radiation-hardened video systems is necessary. Remote VT has been used successfully to find cracks in pressure vessel cladding in PWRs and core shrouds in BWRs and to investigate leaks in reactor and piping components. These visual tests are performed using a wide variety of procedures and equipment. Techniques generally include the use of submersible closed-circuit high-resolution video cameras to examine reactor components. Numerous industrial camera systems are available for this purpose. These systems have video resolutions ranging from 470 to 600 vertical lines on the screen, roughly equivalent to a 640 × 480-pixel count, and most systems typically possess zoom capability to achieve fields of view of 24 mm × 18 mm (0.9 in. × 0.7 in.) or smaller. There is no standard method for visual test lighting. The cameras typically have a pair of spotlights mounted near the lens to provide illumination. The authors are aware of at least one system that has a light-emitting diode (LED) ring light mounted around the lens. The camera is normally manipulated by operators standing on the refueling bridge using an arrangement of poles and/or ropes. The inspection is primarily performed via a live view of the video on a monitor. The video data with an operator voice-over is typically stored digitally as it is taken for later review.

2.1 Standards in Visual Testing

Nuclear utilities today follow guidelines for remote VT found in the Electric Power Research Institute (EPRI) BWR Vessel and Internals Project-03 (BWRVIP-03; EPRI 2005). These guidelines specify that examined surfaces must be clean, and for underwater testing, that the water be clean and clear. The BWRVIP guidelines also describe training requirements for personnel and specify which areas around a weld should be examined, how to measure the sizes of indications found, and how to test the resolving power of the visual equipment used for the test. There are no guidelines dealing with scanning speed or field of view used during the inspection. To test the visual acuity of the camera system and lighting, the EPRI guidelines call for the camera system to image a sensitivity, resolution, and contrast standard (SRCS) before and after the inspection. This SRCS typically contains two perpendicular wires 12 μm (0.0005 in.) in diameter as a resolution calibration standard. If the camera and lighting are sufficient to detect the wires, then the camera system is deemed to have a resolution sufficiently high for the inspection. The very important issue of lighting is also presumed covered by this line detection test.

2.2 Previous Studies on Crack Detection

Few comprehensive studies of the probability of various video systems used for remote VT to detect cracks relative to crack opening displacement (COD) have been published to date. A visual system was used in Sweden to test crack detectability in reactor components, and the reported detectable limit for flaws was 20 μm (0.0008 in.) (Efsing et al. 2001). Useful information on the evaluation of remote VT was found in a recent human factors study performed in Sweden (Enkvist 2003). A series of cracked ceramic specimens, molded to reproduce the surface appearance of a welded region, was examined underwater by 10 operators using a high-resolution 752- × 582-pixel video camera with an 18X optical zoom and lighting provided by two 15-W halogen lamps. Only one viewing angle and a single distance of 200 mm (7.9 in.) from the test samples were used, so the tests were more restrictive than actual field VT. The area inspected by the system at maximum magnification was 47 × 35 mm (1.85 × 1.46 in.), with

a resulting pixel size of 60 μm (0.0024 in.). Cracks larger than 40 μm (0.0016 in.) COD were detected easily, while cracks less than 20 μm (0.0008 in.) COD had, at best, a 20% probability of detection using the "Lenient" grading scale defined by Enkvist (2003).

A study on the detectability of tight thermal fatigue cracks (Virkkunen et al. 2004) under normal inspection conditions was performed using a commercially available remote camera system. The cracks ranged in COD from less than 20 μm to 200 μm (<0.0008 to 0.008 in.). In this study, the camera was focused on an area 60 × 45 mm (2.36 × 1.77 in.). The cracked area was scanned at 2 cm (0.8 in.) per second, the data recorded, and the images later reviewed frame by frame. Identified areas of interest were then re-examined statically with a focal area of 12 × 9 mm (0.47 × 0.35 in.). This careful scanning, evaluation, and re-evaluation showed that the smallest cracks that could be reliably detected were 100 μm (0.0039 in.) COD or larger, and the smallest defects possible to detect were 40 μm (0.0016 in.) COD. The detection rate for cracks smaller than 100 μm (0.0039 in.) COD was approximately 20%.

2.3 Cracks in Reactor Components

To determine if a remote VT system is capable of detecting actual cracks, a discussion of typical service-induced crack dimensions is needed. The primary feature of a crack to be visually detected is its width, or COD. The COD is a function of several factors, some of which are material hardness, applied loads, crack length, residual stresses around the crack opening, and the degree of corrosive attack at the crack opening. The specific variables of most importance to COD depend on the type of crack involved. For instance, literature reports that the width of intergranular stress corrosion cracking (IGSCC) is fairly random and is primarily a factor of how many grain boundaries at the crack opening are affected.

Several hundred cracks of various types and origins in many materials have been characterized and documented in the literature in the United States and in Europe (Ekström and Wåle 1995; Wåle 2006). The results show that the CODs of inservice-generated cracks are highly variable over most crack types and materials, and several outlier sizes were found that increase the range of the datasets. However, it was found that most reported CODs tend to be populated around a mean, or median, crack width. Table 2.1 provides a compilation of COD ranges for various types of service-induced degradation.

Table 2.1 Crack Widths in Stainless Steel Components

	IGSCC SS	IGSCC Ni	IDSCC Ni	TGSCC SS	Thermal Fatigue	Mechanical Fatigue	Hot Cracks
Total Cracks	65	14	14	25	29	15	17
Minimum (μm)	3	4	0	3	5	3	2
Maximum (μm)	160	260	120	500	380	450	250
Mean (μm)	37.7	42.4	33.4	49.9	51.4	79.4	38.6
Median (μm)	30	17.5	21	20	30	16	25
RMS (μm)	47.2	77.8	48.5	110	85.4	144	67.3
Standard Deviation (μm)	28.7	67.7	36.4	99.6	69.3	125	56.8

It is important to note that the median values for these cracks are very tight, with CODs on the order of 16 to 30 μm (0.0006 to 0.0012 in.). The results show that COD is highly variable over all crack types and materials. This presents a significant challenge when attempting to detect cracks using remote video camera systems.

Equally important, the findings also show that COD is largely independent of the crack through-wall depth and crack length. Thus, judging the overall crack depth by COD is not reliable (Ekström and Wåle 1995). Also, one cannot assume that long cracks have a wider COD than short cracks. Therefore, even if the COD is large enough to be detected visually, other volumetric NDE methods must be used to fully characterize the crack boundaries.

Another factor that aids in crack detection is crack tortuosity (a less technical term might be "crookedness") and branching frequency. Crack tortuosity is a measure of the number of bends in the crack per unit length, and branching describes how often the crack branches off per unit length. A perfectly straight crack that does not branch may be more difficult to detect than one that has many bends and branches, as the bends and branches help to distinguish the cracks from innocuous surface features. One crack morphology occasionally seen with thermal fatigue cracking is called "cobblestone" cracking, which consists of several cracks in close proximity. Cobblestone cracking affects a region and creates Crack shape versus crack type is shown in Table 2.2 while the number of turns per mm vs. crack type is shown in Table 2.3.

Table 2.2 Crack Shape Versus Crack Type

	IGSCC SS	IGSCC Ni	IDSCC Ni	TGSCC SS	Thermal Fatigue	Mechanical Fatigue	Solidification Cracking
Total Cracks	39	4	15	15	28	14	5
Straight, %	64	75	85	60	44	100	80
Winding, %	26	25	15	13	33	0	20
Bent, %	10	0	0	13	0	0	0
Branched, %	0	0	0	13	0	0	0
Cobblestone, %	0	0	0	0	22	0	0

Table 2.3 Number of Turns per Millimeter Versus Crack Type

	IGSCC SS	IGSCC Ni	IDSCC Ni	TGSCC SS	Thermal Fatigue	Mechanical Fatigue	Solidification Cracking
Total Cracks	38	3	5	5	14	4	14
Minimum	4	16	2.7	5	1	1	1
Maximum	40	128	8.5	16	12	6	46
Mean	12.7	65.7	5.7	10.3	3.61	4	12.6
Median	9.9	53	7	8	3	4.5	9.5
RMS	15.2	80.5	6.14	11.2	4.54	4.53	17
Standard Deviation	8.51	57.1	2.55	4.88	2.87	2.45	11.8

2.4 Cracks in Components

When a crack is detected in a component, several issues need to be addressed such as the structural significance of the crack, continued operation, and inspection frequency. Many components can contain relatively long cracks without significantly affecting plant safety. The effect of a flaw on structural integrity and its acceptability for continued operation is based on the structural mechanics of the system and the theoretical crack growth rate of the degradation mechanism. Each individual reactor typically produces a set of flaw tolerance guidelines for each system based on the stresses and actual configuration of individual components.

Fracture mechanics analyses have been performed relative to postulated critical flaw sizes for BWR reactor vessel internal components. PNNL has analyzed representative acceptable lengths of flaws detected by VT examinations in BWR reactor vessel internal components. VT methods applied for inservice inspection should detect flaws before they grow to a critical size with a high level of reliability. The reviewed documents included both BWRVIP reports prepared by EPRI (EPRI 2003, 2005) and calculations from two representative BWRs.

The BWRVIP documented evaluations were based on ASME Section XI approaches that were developed originally for flaws in stainless steel piping. Although some of the components were not strictly ASME Code pressure boundary components, the calculational methods have been reviewed and accepted by the NRC. Given that VT examinations provide no measurements of flaw depth dimensions, all calculations conservatively assumed that the unmeasured flaw depths extended through the entire wall thickness.

Limit load calculations have evaluated flaws in stainless steel base metal and in welds made without the use of welding fluxes. Consistent with ASME Section XI, conservative calculations have been performed for flux-type welding processes (shielded metal arc or submerged arc). These calculations accounted for reduced material toughness (Z factor approach) and included stresses from thermal expansion bending moments as a primary stress that can contribute to unstable crack growth.

The acceptable flaw lengths have accounted for flaw growth (due to stress corrosion cracking or fatigue) between successive inspections and have addressed uncertainties in VT measurements of flaw lengths. These adjustments have been relatively small. Flaw growth rates have been taken to be 25.4×10^{-5} mm/hr (10^{-5} in./hr). This gives 4.45 mm/year (0.175 in./year) increase in the flaw length, which accounts for the growth from both ends of a through-wall crack.

The calculations address two concerns. The primary concern has been that of unstable crack growth by ductile tearing. The second concern has addressed the leakage flow rate through the crack. This second calculation has predicted leakage flows that are small relative to the flow required for the component to perform its intended safety function.

Plant-specific calculations of acceptable flaw lengths are proprietary. The representative examples analyzed by PNNL are given in Table 2.4. Even though a limited number of examples were analyzed, the results nevertheless show some interesting trends, as discussed in the following paragraphs.

Table 2.4 Examples of Calculated Lengths for Acceptable Flaws Detected by VT Examinations

Component	Material	Diameter	Weld Length	Thermal Expansion Stress	Total Stress	Acceptable Flaw Length	Acceptable Flaw Length Fraction of Weld Length
Core Shroud – Vertical Weld	304L		251 cm (98.8 in.)	-	3.0	162 cm (63.6 in.)	0.64
Jet Pump – Thermal Shield to Elbow Weld (Limit Load Failure)	304	10 in., Sch 40	~ 79 cm (31 in.)	-	-	36.3 cm (14.3 in.)	0.46
Jet Pump – Thermal Shield to Elbow Weld (Onset of Fatigue Crack Growth)	304	10 in., Sch 40	~ 79 cm (31 in.)	-	-	14.6 cm (5.75 in)	0.19
Core Spray Line – Non Flux Weld	304	13 cm (5 in.)	~ 38 cm (15 in.)	23 MPa (3.3 ksi)	32 MPa (4.6 ksi)	25.0 cm (9.86 in.)	0.66
Core Spray Line – Flux Weld	304	13 cm (5 in.)	~ 38 cm (15 in.)	220 MPa (32 ksi)	234 MPa (34 ksi)	3.30 cm (1.3 in.)	0.09
Core Spray Line – Non Flux Weld	304	13 cm (5 in.)	~ 38 cm (15 in.)	23 MPa (3.3 ksi)	32 MPa (4.6 ksi)	18.8 cm (7.42 in.)	0.49
Core Spray Line – Flux Weld	304	13 cm (5 in.)	~ 38 cm (15 in.)	64 MPa (9.3 ksi)	83 MPa (12 ksi)	15.1 cm (5.95 in.)	0.40
Sparger– Example 1	304	13 cm (5 in.)	~ 28 cm (11 in.)	9.6 MPa (1.4 ksi)	17 MPa (2.5 ksi)	16.5 cm (6.48 in.)	0.59
Sparger– Example 2	304	13 cm (5 in.)	~ 28 cm (11 in.)	9.6 MPa (1.4 ksi)	17 MPa (2.5 ksi)	16.1 cm (6.33 in.)	0.58

Vertical Weld of Core Shroud – This calculation conservatively takes no credit for the integrity of the circumferential welds (360-degree through-wall cracking) such that each shell course was treated as a separate component. The most embrittled shell course was evaluated for a through-wall vertical (axial) crack based on a fracture toughness of 165 MPa-$m^{1/2}$ (150 ksi-$in.^{1/2}$). Both normal operating and faulted conditions were addressed that gave a relatively low governing hoop stress of 21 MPa (3 ksi). The acceptable flaw length was calculated to be 162 cm (63.6 in.) compared to the 251 cm (98.8 in.) vertical length of the shell course.

Jet Pump Weld of Thermal Shield to Elbow – This calculation for the second sample BWR addressed cracking of the weld in the jet pump that joins the thermal shield and elbow. A circumferential crack was assumed to extend through the full wall thickness. Two allowable flaw lengths were calculated. A length of 14.6 cm (5.75 in.) assumed that the onset of fatigue crack growth was the governing consideration. A

larger flaw length of 36.3 cm (14.3 in.) was established for the assumption that limit load failure was the sole consideration for structural integrity.

Core Spray Line – These calculations, performed for the two sampled BWRs, which are for 13-cm (5-in.) outside diameter Schedule 40 stainless steel piping (EPRI 2005) and assumed a through-wall circumferential crack. Separate calculations were performed for the two BWRs and for flux welds versus non-flux welds. Acceptable flaw lengths ranged from 3.3 cm (1.30 in.) to 25.0 cm (9.86 in.).

Sparger – These calculations performed for the two BWRs were for 8.9 cm (3.5 in.) outside diameter Schedule 40 stainless steel piping (EPRI 2005) and assumed a through-wall circumferential crack. The acceptable flaw lengths were calculated to be 16.0 cm (6.33 in.) and 16.5 cm (6.48 in.) for the two BWRs, respectively.

The review addressed a sample of BWR reactor internal components and considered locations where cracking has been observed or has a potential to occur. The calculations of acceptable crack lengths have been based on conservative considerations including an assumption of through-wall crack depths for the flaws as detected by VT examinations, application of ASME Code safety factors, and the assumption in some cases of lower-toughness flux-type welds. Even with these conservative assumptions, most of the calculated crack lengths were several inches long, although the most limiting example had a calculated flaw length of 3.3 cm (1.30 in.).

It should be noted, however, that there have numerous reports of cracking in certain components of the jet pump assembly and for some component areas, the acceptable crack lengths are in the mid-range of cracks described in this report (i.e., at the lower end of the capabilities of the equipment). In addition, UT is not a viable option in some of these locations either because of geometry or because of the high number of locations that require inspection. Therefore, it is critical to perform VT inspections of the highest quality.

2.5 Factors Influencing Crack Opening Displacement

For thermal and mechanical fatigue cracks, the largest factor governing the crack COD is the stress acting perpendicular to the crack opening (Yoneyama et al. 2000; Kim et al. 2003; Xaio et al. 2002). According to the Westergaard stress function, the maximum COD of a semicircular crack is given by Chen et al. (1996) as

$$COD = \frac{4a\sigma}{E} \tag{2.1}$$

where a is the crack depth (and one half the crack length), σ is the stress on the material, and E is Young's modulus. In a fatigue crack, the COD strongly depends on the state of the material when the crack is measured. If a mechanical fatigue crack is examined when the material is not in tension, the crack can be closed entirely. Without a stress σ, the theoretical COD is zero. Often, the only stress available to hold a fatigue crack open is the residual stress causing the crack formation or resulting from fabrication processes. As the residual and other stresses at a given point are not generally known, one cannot use the COD to predict the through-wall depth of a crack.

It is worth noting that nuclear reactor components are examined during outages when systems are not at operating temperature and pressure. Some of the main sources of stress are not present when the components are examined. With all of the pressure relieved and the differential temperatures across components eliminated when the reactor is shut down, the COD of the cracks in the reactor will most likely decrease to a minimum size.

The factors influencing the CODs for stress corrosion cracks are more complex than for fatigue cracks. Stress corrosion cracks (SCC) form because of an interaction between a sensitized material, a corrosive environment, and stresses in the material. When SCC occurs, the opening size may depend on the susceptibility of the material and the residual stresses around the crack. A stress corrosion crack can have a very small COD if one grain boundary is affected in a lightly susceptible material or a very large COD in a very susceptible material when several surface grains are dislodged from the crack (Garcia et al. 2001). A highly sensitized material can form many SCCs in the same area, which may then link up and form a crack with a large COD. A less sensitized region will have fewer and tighter SCCs. There is no reliable way to gage the depth of a SCC based on its COD.

2.6 Primary Factors in Crack Detection

The challenge faced by inspectors using standard and remote VT is to find and correctly identify cracks on the surfaces of nuclear components. This problem can be broken down into three primary parameters—contrast, recognition, and discrimination.

For crack detection to occur, sufficient contrast must exist between a crack and the background. A high-contrast crack is easily seen and easier to identify. A low-contrast crack is easy to miss or to confuse with other features. Any factor that increases the contrast between the crack and the background will improve detectability, while anything that decreases the contrast will reduce the detectability.

When one is discussing contrast as it relates to video cameras and other automated systems, it is important to understand how the cameras capture and transmit the image to the inspector. High-quality video cameras and digital cameras have 8 bits of dynamic range. This means that each color that the camera collects has 256 levels of brightness. For a black-and-white camera, this translates into 256 shades of gray. A human eye can distinguish between 100 to 200 levels of grey, which is less than the camera systems. Figure 2.1 shows a gray box (grayscale level 146 of 256) with a series of vertical lines arranged inside. Each line is progressively one grayscale level (out of 256) darker than the previous, with an additional line on the left, which is 210 levels separated from the background. Figure 2.1 shows that at less then 10 levels of separation from the background line, detection is very difficult. At between 10–20 levels separation from the background, the lines are faintly detectable, and above 20 levels separation from the background, the lines are clearly visible. It should also be noted that the higher the system acuity, the higher the contrast in the image. When the image is slightly blurred, the overall contrast levels drop. The blurred lines are still detectable but are slightly more difficult to see because of the lower contrast.

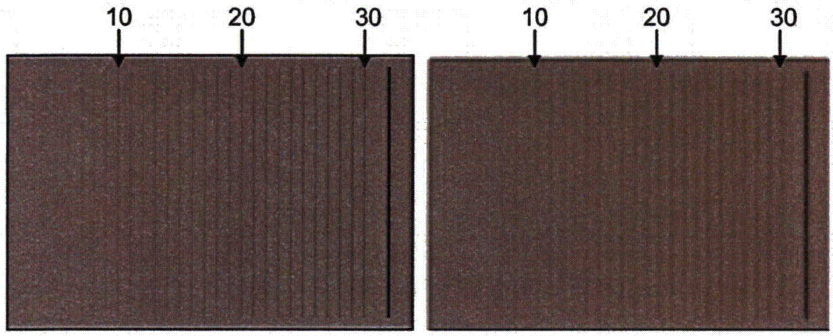

Figure 2.1 Relationship of Line Visibility to Contrast Between Line and Sharpness of Background and Image

For crack recognition to occur, the system also needs sufficient visual acuity to accurately image the morphology of the crack. Cracks come in a variety of shapes, depending on the type of crack and the material. In general, cracks have a slightly-to-very zigzagged appearance, with or without branching. A system interrogating a surface needs be able to distinguish these characteristics to allow the inspector to identify the detected image as a crack.

An example of the difference between recognition and detection and how recognition is affected by visual acuity is shown in Figure 2.2. The effects of reduced contrast and reduced acuity are shown in Figure 2.3.

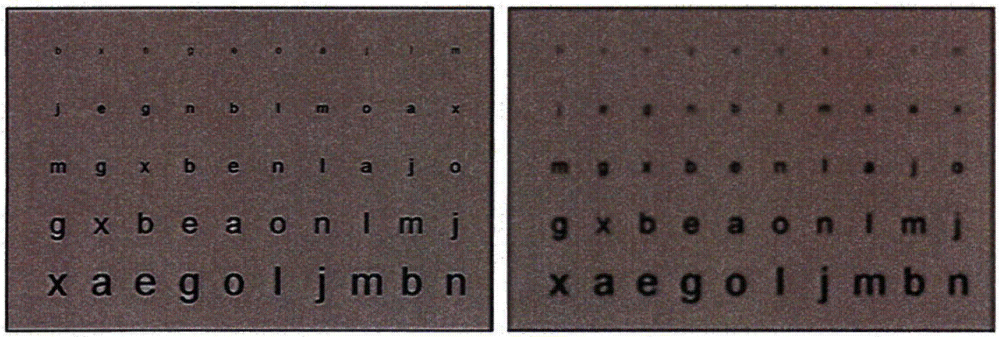

Figure 2.2 Recognition of High-Contrast Letters as a Function of Letter Size and Image Sharpness

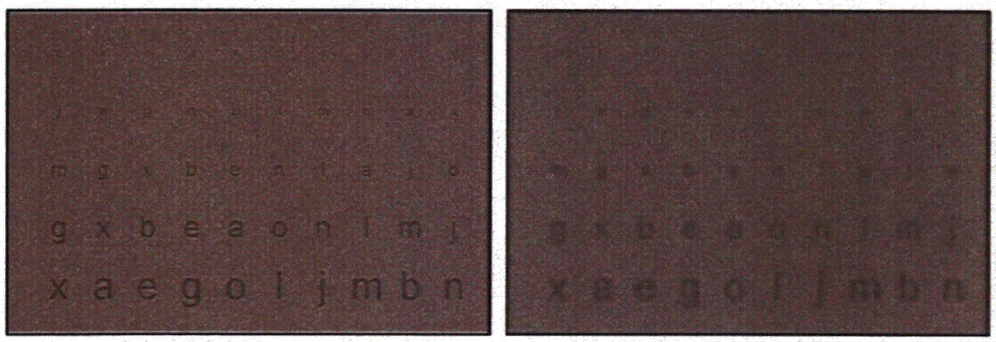

Figure 2.3 Recognition of Reduced-Contrast Letters as a Function of Letter Size and Image Sharpness

Finally, if the crack is detectable and recognizable, the crack must be distinguishable from the surrounding innocuous features such as geometry and scratches. Common issues that can mask a crack include machining marks, grinding marks, scratches, weld conditions, corners and joints, and other geometrical conditions. A crack surrounded by parallel scratches or machining marks can be much more challenging than a crack on a smooth surface. A crack along a weld may be difficult to separate from the weld root or crown, and a crack in a tight corner may be difficult to detect. Geometry can provide other effects such as casting shadows over areas of interest.

The parameters described in this report will be described in terms of how they affect the three primary factors of contrast, recognition, and discrimination.

2.7 Determining Visual Acuity

Any system used in VT, ranging from the naked eye to a digital closed-circuit television (CCTV) system, will have a measurable visual acuity. The visual acuity of a system has four pseudo-independent measures (De Petris and Macro 2000):

- visible minimum – the smallest dot the system can detect
- separable minimum (resolution) – the smallest separation between two lines the system can detect
- visual acuity by Vernier – the ability to perceive spatial variation between two objects
- readable minimum (recognition capability) – the ability to recognize complex shapes such as letters or numbers.

These visual acuity parameters describe what a system can detect and discern. A system with a detection limit of 10 μm (0.0004 in.) and a resolution limit of 30 μm (0.0012 in.) at a given distance can "see" a line 10 μm (0.0004 in.) wide on a sheet of paper but cannot resolve a 10-μm (0.0004-in.) gap between two 10-μm (0.0004-in.) lines. A letter or number will appear to be a dot if it is larger than the visible

minimum of a system but below the readable minimum of the system. The letter will be identifiable only when it is above the recognition capability of the system.

A human eye with 20/20 vision is able to resolve features as small as 75 μm (0.003 in.) in size at a distance of 25 cm (10 in.) (Allgaier et al. 1993). This limit is based on the density of rods in the retina of the eye and on the diffraction limit imposed by the size of the eye. The eye is also, however, able to detect features too small to be accurately resolved. It is possible under perfect conditions to detect a crack with a surface width, or COD, as small as 10 μm (0.0004 in.) on a mirror-polished surface (Allgaier et al. 1993). The minimum detectable COD becomes much larger if the surface is rough or not perfectly clean. These limits do not account for factors such as scratches, machining marks, or any camouflaging effects offered by a macroscopic feature such as a weld root or crown.

The image sharpness produced by mechanical visual systems such as still and video cameras can be described in terms of their modulation transfer function (MTF). The MTF is a measure of the detected versus the actual contrast ratio as a function of the spatial frequency of the indications. For example, a camera will generally show nearly 100% contrast on two black lines on a white background when the lines are far apart (low spatial frequency); however, if the lines are very close together (high spatial frequency), the system can blur the lines and the spaces between the lines together, reducing the contrast and thus reducing the MTF. Measuring the MTF of a system as a function of spatial frequency is a very reproducible and objective way to measure the visual sharpness of a camera system.

A resolution test is another common technique used to characterize the visual acuity of a system. A resolution test determines the smallest distance between two lines that can be discerned by the system. A resolution target generally has several sets of parallel or converging lines with notations on how many lines per millimeter are present at each point. Performing a resolution test consists of making an image of a standard resolution target and determining the point at which the system can no longer separate the lines. The main problem with resolution tests is that they rely on the observer to determine which lines are separable and which are not, adding an element of subjectivity to this measurement. However, a resolution test has the advantage of being faster and easier to administer than a test of system MTF. Examples of commercially available resolution targets include the Institute of Electrical and Electronics Engineers (IEEE) Resolution Target, which conforms to the standard STD 208-1995, "Measurement of Resolution of Camera Systems," the 1951 U.S. Air Force Resolving Power Target and the International Organization for Standardization (ISO) Camera Resolution Chart. The details of which targets conform to which standard can be found in Sine Patterns L.L.C. (2004).

As the 1951 U.S. Air Force resolution target has been used to test the various cameras used in the PNNL experiments for the parametric and laboratory tests, it bears further description. The 1951 Air Force resolution target consists of a series of increasingly narrow horizontal and vertical lines. The lines are arranged in groups made up of six elements. A sample image of a 1951 Air Force resolution chart is shown in Figure 2.4.

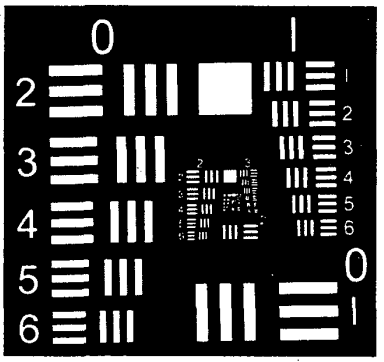

Figure 2.4 Sample Image of a 1951 U.S. Air Force Resolving Power Target

Each element is smaller than the previous by a factor of the sixth root of two (0.891). This progression is designed so that the size of the lines is halved (and the number of lines per millimeters is doubled) every six elements. Thus, each group of six is one half the size of the proceeding group. The number of line pairs per millimeter for a series of groups and elements is given in Table 2.5.

Table 2.5 Number of Lines per Millimeter by Group and Element in a 1951 U.S. Air Force Resolving Power Target

	Group Number					
Element	**0**	**1**	**2**	**3**	**4**	**5**
1	1.00	2.00	4.00	8.00	16.00	32.00
2	1.12	2.24	4.49	8.98	17.96	35.92
3	1.26	2.52	5.04	10.08	20.16	40.32
4	1.41	2.83	5.66	11.31	22.63	45.25
5	1.59	3.17	6.35	12.70	25.40	50.80
6	1.78	3.56	7.13	14.25	28.51	57.02

The maximum visual acuity of an analog or digital video system can be described by comparing the native resolution of the system to the size of the area on which the system is focused. This measure of acuity assumes perfect optics and a perfect electronic capture of the image. Using this method, a 1-megapixel (1200 × 800 pixels) camera that can focus on an area 75 mm × 50 mm (3 in. × 2 in.) would have a pixel size of 0.0625 mm/pixel (0.0025 in./pixel). Any indications that fall below this size would be pixilated and recorded as a lower-contrast shadow in the larger pixel, as the contrast from the indication is averaged with the background in the pixel. The color and shading of the pixel is dependent on the contrast between the indication and the background and on the MTF of the camera. With analog and digital video systems, one needs, as a theoretical minimum, at least one pixel (or line) width between two lines to resolve them, assuming the lines are perfectly aligned with the camera. In practice, this corresponds to at least 1.4 pixels between two lines to always be able to resolve them, regardless of the angle and orientation of the lines.

Another important variable in visual acuity is the speed at which the imaging detector is moving over the inspected area. The term *kinetic vision acuity* is used for the acuity of a given system when scanning a moving target. The loss of visual acuity as a function of scan speed is highly dependent on the technology used to capture the images. A high-speed film camera can produce sharp images of a bullet in flight, while a poor video system can show noticeable blur at slow scan speeds. A captured image picture is typically sharper when the camera is stationary (system normal visual acuity) over a zone as opposed to moving (system kinetic visual acuity).

2.8 Brightfield and Darkfield Imaging

Two ways to use light to examine features on the surface are using reflected darkfield and reflected brightfield imaging. The most common way to image a surface for visual testing is with brightfield imaging. Brightfield imaging is performed by directly illuminating the surface. The surface will be a bright background with features appearing as bright or dark depending on their reflectivity or color relative to the background. With brightfield imaging, cracks look like a dark indication against the brighter background. Scratches can appear as dark or light indications depending on their depth and the angle of illumination.

Darkfield illumination is performed when one shines light on the inspected surface at an oblique angle. Absent discontinuities on the surface, none of the light should reach the camera, and the background will appear dark. Surface features such as cracks and scratches will appear as bright indications, as the light reflects off the indications and reaches the camera. Darkfield imaging can be a very powerful tool in crack detection under good conditions and is commonly used to look for cracks in airplane wing panels and to resolve other inspection issues.

Examples of how one would illuminate a surface with dark and brightfield lighting are shown in Figure 2.5. Examples of a crack illuminated using both darkfield and lightfield illumination are shown in Figure 2.6. In the darkfield-lit image, the crack shows up clearly as a bright indication. The scratches are also well imaged by the darkfield illumination. The brightfield image clearly shows the crack as a dark image against the bright background.

Darkfield lighting is primarily only useful on smooth and flat surfaces. Curved specimens, welded specimens, and machined surfaces make darkfield illumination challenging. For this reason, all remote visual testing is performed as brightfield examinations. Direct visual inspections where one has use of a flashlight can be and often are performed using darkfield imaging as an adjunct to brightfield examinations.

If light is coming from certain angles relative to the surface, the crack can produce both brightfield and darkfield effects. An example of this effect is shown in Figure 2.7. The edge of the crack can reflect light and produce a bright indication, and the center of the crack will still produce a dark indication relative to the background. This combination of brightfield and darkfield effects can be both an aid and a hindrance for detecting a feature. If the feature is large relative to the visual acuity of the system, the two forms of lighting can help brightly outline a dark feature, which often makes the feature very easy to detect. If the feature is small relative to system visual acuity, then there is a danger the brightfield and darkfield effects will overlap in the image and cancel each other out, hiding the feature.

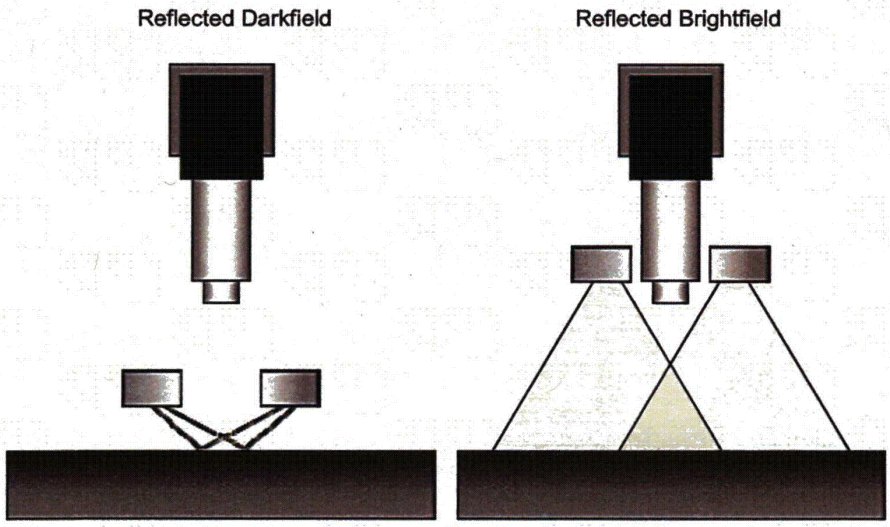

Figure 2.5 Lighting for Brightfield and Darkfield Imaging

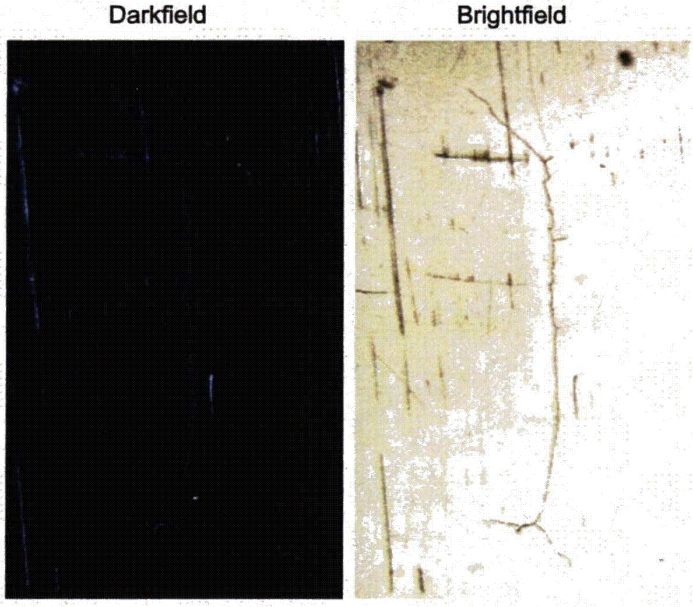

Figure 2.6 Crack with 12-μm Crack Opening Depth Imaged Using Both Darkfield and Brightfield Illumination

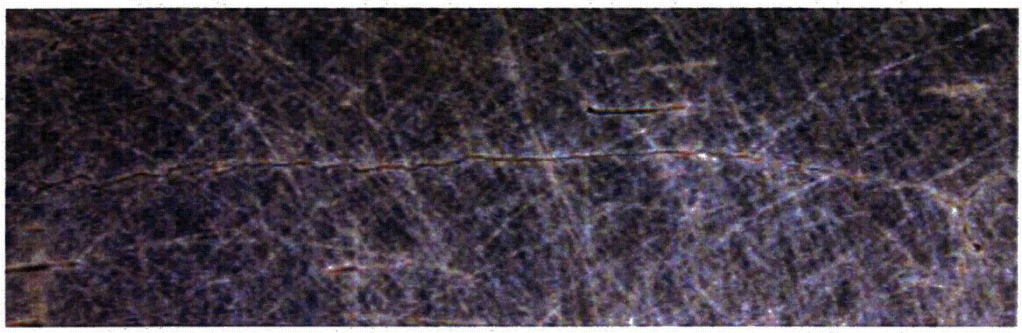

Figure 2.7 Simultaneous Brightfield and Darkfield Effects Produced by Lighting at Off Angle

2.9 Specular and Diffuse Reflection

Light reflection from a given surface has two modes, specular and diffuse. In specular reflection, light reflects from the surface at the same angle as the angle of incidence. In diffuse reflection, the light reflected from the surface has no relation to the angle of incidence and is emitted isotropically. The two modes of reflection are shown in Figure 2.8.

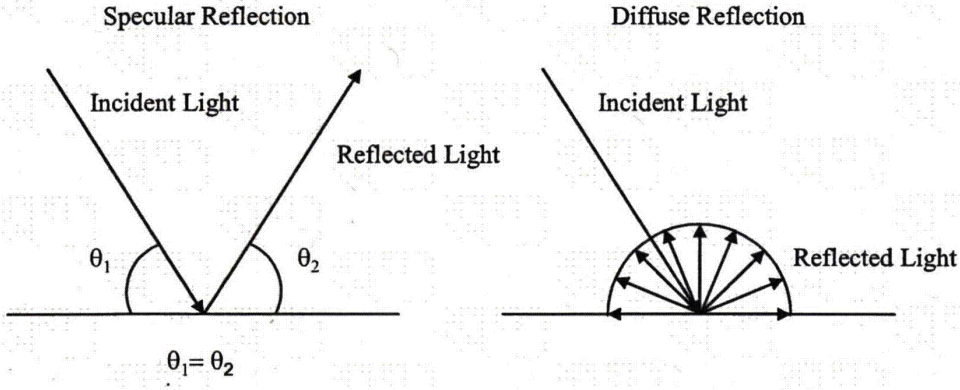

Figure 2.8 Specular and Diffuse Reflection. When light strikes a highly specular surface (left), the light is reflected away at the incident angle. When light strikes a diffusely reflecting surface (right), it reflects isotropically.

For many surfaces, one finds that some of the light reflects specularly and some of the light reflects in a diffuse fashion. This condition is often seen on a slightly oxidized stainless steel surface or a rough metallic surface. One can also find this condition on a scratched surface that would normally be very specular. An important measurement is the ratio between specularly reflected light and diffusely reflected light. For a very diffusely-reflecting surface with virtually no specularity, such as a typical piece of paper, the amount of light reflected at the specular angle will be equal to the light reflected at all angles, giving a ratio of 1. For a highly specular surface such as a mirror, the ratio of specular to diffusely reflected light should be very high.

3 Experimental Procedures

PNNL conducted a series of experiments on cracked stainless steel samples to test the abilities of mechanical systems to image cracks and discriminate between cracks and innocuous surface features. Both the parametric study and the laboratory tests used a series of welded stainless steel samples built to mimic unoxidized BWR core shroud surface conditions.

3.1 Parametric Study

The parametric study was designed to test the effects of several variables on the ability of a mechanical system to image a crack on a metal surface. The parameters specifically examined in this study are the following:

- inspection-dependent parameters
  - camera resolution/magnification
  - lighting techniques
  - scanning speed
- sample-dependent parameters
  - crack opening displacement
  - surface specularity
  - surface features

3.2 Cameras and Lights

The parametric study experiments used three cameras. The largest part of the work was performed using a Lightwise ISG CMOS Firewire video camera with 1.3-megapixel resolution and a Navitar 12X automated zoom lens. Using a 1951 U.S. Air Force resolution target, the maximum resolution for the system with the standard lenses was 90.51 lines per millimeter. The camera was typically mounted on a peg-track scanner that allowed for very precise camera positioning and control. The system is shown in Figure 3.1. This camera was very useful in examining the influence of magnification, crack size, lighting style, and surface conditions.

The lights used in the parametric studies included incandescent and LED spotlights, an LED diffuse ring light, and a diffuse on-axis light™. The spotlights are standard spotlights used for different applications. The diffuse ring light is very similar to the ring lights used in microscopy or macro photography but with a layer of frosted glass in front of the lights. The diffuse on-axis light is designed to provide very flat diffuse lighting on a surface, allowing for good imaging of features on items with highly specular surfaces such as compact disks, glass, and polished metals. The various lights are shown in Figure 3.2. Figure 3.3 shows some of the capabilities of the camera, lens, and lighting systems on a familiar test subject. The diffuse axial provides the flattest and most even lighting on the subject. The diffuse ring light provides even illumination but with some glare. The spotlight produces a great deal of glare, and much of the dime is not well imaged.

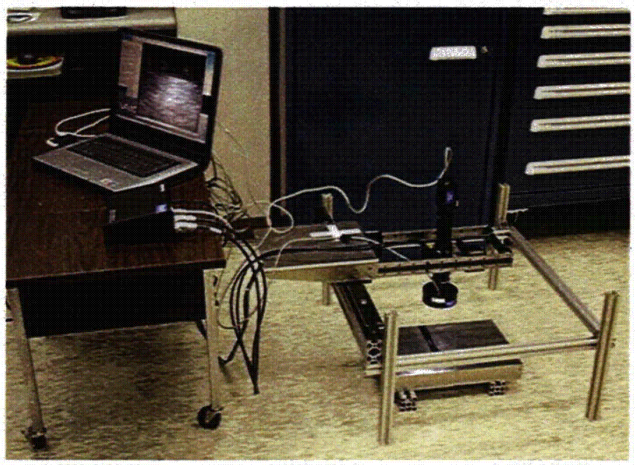

Figure 3.1 Visual Testing Apparatus and Sample

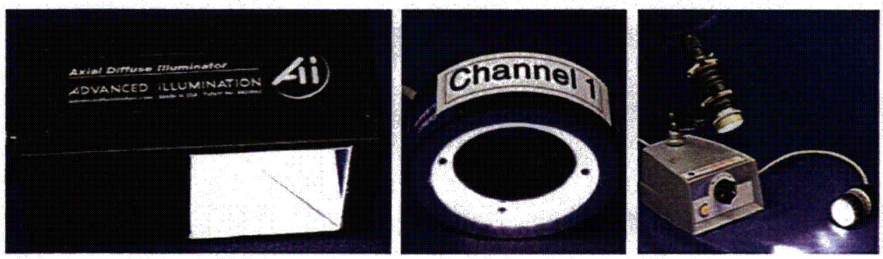

Figure 3.2 Lights Used in Visual Testing Experiments. Diffuse on-axis light on the left, ring light in the middle, and spot lights on the right.

Diffuse on Axis Diffuse Ring Light Spot Light

Figure 3.3 Dime Illuminated Using Three Lighting Techniques

The other cameras used for the parametric study were the two radiation-hardened cameras used in the laboratory studies and are detailed in the next section. They were useful in determining the effects of scanning speed and camera angle.

3.3 Specularity Measurements

Specularity measurements were made on two cracked samples. These measurements were taken to determine the effects of the different lighting techniques on surfaces with varying degrees of polish and shininess. The specularity measurements define the degree of shininess with objective measurements and allow for comparisons to materials with similar measured properties.

The measurements were made using a 12-in.-diameter integrating sphere and a helium neon laser (SpectraPhysics, Model 145-02, Class IIIb). The setup is shown in Figure 3.4.

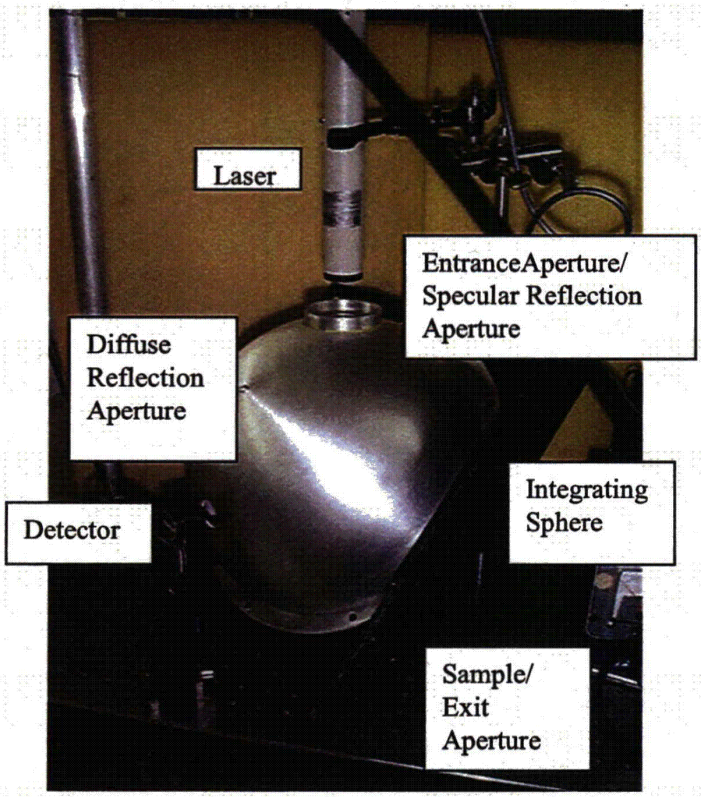

Figure 3.4 Experimental Setup for Specularity Measurements